Assessment of empirical models to estimate UV-A, UV-B and UV-E solar irradiance from GHI

Agustín Laguarda[1] and Gonzalo Abal[1,2]

[1] Laboratorio de Energía Solar, Facultad de Ingeniería, Montevideo (Uruguay)

[2] Laboratorio de Energía Solar, CENUR LN, Salto (Uruguay)

Abstract

Exposure to the UV solar irradiance reaching the ground has an important impact on human health, vegetable growth and the degradation processes of several materials. As a first step of a larger project aiming to characterize typical UV exposure potential over the territory of Uruguay, three families of simple UV irradiation models based on GHI and atmospheric Ozone information are trained and evaluated using data from three sites (one of them in King George's Island, Antarctica). The air mass, clearness index and satellite-derived (OMI/TOMS) daily Ozone column are used as predictors to estimate 15-minute irradiation in the UV-A, UV-B, and UV-Erithemic bands. All models are locally adjusted and perform similarly. The best model predict UV irradiation with typical uncertainties between 6 and 7% and small but consistent negative biases. The use of a constant UV fraction is considered inadequate in the region for most applications.

Keywords: UV model, UV-A irradiation, UV-B, Erythema.

1. Introduction

An accurate knowledge of the ultraviolet component of solar irradiation (the spectral band below 400 nm), incident at the earth surface is important due to its wide range of effects, in agriculture, degradation of materials and especially in human health. Solar UV irradiance is usually divided in sub-bands according to its effects on biological tissues (WMO, 2014): UV-A (315-400 nm) responsible for skin aging, UV-B (280-315 nm) which can cause DNA damage or sun burns, and UV-C (100-280 nm) which can be highly toxic but is fully absorbed by the atmosphere and will not considered in this paper. Erithemic UV irradiance (UV-E) is defined weighting UV with an average human skin response (ISO17166, 1992). The UV index, used world-wide to communicate the UV-related risk level to the general public, is proportional to UV-E irradiance. According to the American Cancer Association, skin cancer is the most common type of cancer in young adults and 264 persons per day are diagnosed in the USA and about 10 % of these are terminal (ACS, 2019). In the region of interest in this paper, Uruguay's territory, skin cancer is also a relevant problem with a high mortality rate of 1 person every 4 days. However, the average distribution of UV irradiation has not been mapped yet over this area. Since UV irradiation is affected by large spatial and temporal variations, depending on latitude, solar elevation and atmospheric local conditions (Foyo-Moreno et. al, 1997) detailed local studies are necessary. Reliable, long-term local UV irradiance measurements are scarce. However, since global horizontal irradiance (GHI) is a widely measured variable, it is desirable as a first step to have an accurate model to obtain UV irradiance from GHI, with known uncertainty. As a second stage, climatological information on typical UV irradiation doses and spatial distributions can be obtained using

long term GHI information generated by satellite (Alonso-Suárez et al., 2012; Laguarda et al., 2018). In this paper, the first stage of this project is addressed.

A frequent approach to UV modeling consists in a two-step process where UV is estimated under cloudless skies and a UV cloud modification factor ($CMF_{UV,}$ the ratio between the UV irradiation and the UV irradiation under clear sky) is defined. This approach requires an accurate clear sky radiation model using, for example, radiative transfer calculations. The CMF_{UV} can be empirically related to a broadband CMF (Calbó et al., 2005). For instance, Foyo-Moreno et al. (1998) proposed an all-sky model based on a fitted UV clear-sky model obtaining negligible relative Mean Bias Deviation (rMBD) and a relative Root Mean Square Deviation (rRMSD) of 2.3% for Granada, Spain at hourly level in the 290–385 nm spectral range. Indicators are expressed as relative to the average of the measurements. Murillo et. al (2003) applied and adjusted the same model for two different sites in Spain at the hourly level, obtaining rRMSDs in the range 7.7 to 9.5%. An adaptation of this last model, including Ozone information, is used for the UV-E band in (Foyo-Moreno, 2007) reporting rRMSDs under 18% using 30-minute data for seven sites in Spain. A similar approach for daily UV-E radiation is used in (Lindorfs et. al 2007), obtaining estimates with rRMSDs between 7% and 22% for four locations in Northern Europe at hourly level. A general description of many other models of this class can be found in (Calbó et al., 2005).

After implementing some CMF models, we found in general poor performance, probably related to the use of UV clear-sky models as an intermediate step to obtain all-sky UV. A more direct approach is to use empirical models to estimate directly the UV fraction (f_{UV}, defined as the ratio between UV and GHI) or, alternatively, the UV hemispherical Transmittance ($T_{UV,}$ defined as the ratio of UV at horizontal ground level with UV incident on a horizontal plane at the top of the atmosphere). These quantities can be modeled as a function of a few relevant variables, such as air mass (m), clearness index (k_t) or Ozone concentration, [O_3] (Foyo-Moreno et.al 1998; Cañada et.al, 2003; Martin and Goswami, 2005; Martínez, 2007). Under this approach, cloud effects are directly taken into account through the clearness index. For instance, Foyo-Moreno et al. (1998) proposed an exponential parametrization for T_{UV} as function of the clearness index (k_t) and relative air mass m (Young, 1994) and obtained UV irradiance estimates (290–385 nm) with a rMBD of 1.6% and a rRMSD of 8.3 % at hourly level in Granada, Spain, while Murillo et. al (2003) used the same model in Córdoba and Valencia, Spain obtaining rRMSDs in the range 6 to 9%.

In this work, three families of empirical UV fraction models are we implemented and evaluated regarding UV irradiance in each of the three bands UV-A, UV-B and UV-E. The variables m, k_t and [O_3] are used as predictors. In Section 2 the data used for training and assessment and the models structure and training procedure are described. In Sec. 3 the results are discussed including a detailed study of the model's performance. Finally, in Sec. 4 the conclusions are presented.

2. Data and models

2.1 Data description

Three independent GHI and UV ground data sets are used (see Table 1) to assess the models. Two of them correspond to different time periods and instruments at sites in northern

Uruguay (labeled LES and DNM) and the third (BCA) has been obtained by our lab in a summer campaign in the Uruguayan Antarctic Scientific Base at King's George Island, located close to the Antarctic Circle. At the LES and BCA sites, UV-B irradiance was measured by a Kipp & Zonen UVS-T-B radiometer and the UV-A and UV-E were measured simultaneously by a Kipp & Zonen UVST-AE radiometer. Both instruments have internal temperature control and are maintained at 25 ºC. At the LES site GHI irradiance was obtained by Kipp & Zonen CMP10 (secondary standard class) pyranometer and the instruments received daily maintainance, so this data is considered of the highest quality. At the BCA site GHI was measured with a Licor radiometer 200R, preferred due to its better performance under high winds and frequent snow events. All instruments have calibrations traceable to the World Radiation Center in Davos and all data-sets are integrated at 15-minute level (if there are at least 10 1-minute data points in each interval) to smooth out non-typical transient effects. The DNM data set was obtained by the local meteorological service. GHI was measured by a Kipp & Zonen secondary standard CM11 pyranometer and the UV-B and UV-E data were obtained from a Yankee Environmental Systems UVB-1 radiometer. This data was originally registered at 15-minute intervals, as the average of instantaneous readings every 10 seconds for GHI and 1 minute readings for UV-B. The time periods and locations of all datasets are summarized in Table 1.

Daily information of [O_3] from the Total Ozone Mapping Spectrometer or TOMS-EPL3 (TOMS, https://disc.gsfc.nasa.gov/datacollection/TOMSEPL3_008.html) was used up to September 2004 and information fron the Ozone Mapping Instrument or OMI/Aura (Pawan, K. Bhartia, 2012, https://aura.gsfc.nasa.gov/omi.html) was used since then. In both cases the highest quality data set available was used.

Table 1: Details for the data used in this work. Latitude and longitude are in decimal degrees. Site elevation is above the mean sea level. The column labelled ΔT indicates the time period between consecutive data values. The last three columns show the number of diurnal data records (UV-GHI pairs).

Site code	Lat. (º)	Lon. (º)	Elev. (m)	period	ΔT (min.)	UVA	UVB	UVE
LES	-31.28	-57.92	56	09/2015 - 08/2018	1	44159	27017	44219
DNM	-31.44	-57.98	41	09/1997 - 11/2003	15	--	101640	101666
BCA	-62.18	-58.91	18	12/2016 - 04/2017	1	5824	6898	6923

A quality checking of the data is performed: Only data with solar altitude above 7º is used. Clearness index (k_t) must be under 1.1, allowing overirradiance events. Also, all data is visually checked, and reasonable upper limits are set to each band UV fractions. Finally, for UV-B and UV-E data sets, only data with simultaneous available [O_3] information is considered.

Fig.1 shows the behavior of the UV fractions of solar global irradiance, f_{UVA} and $f_{UVB,}$ with k_t, m and [O_3] using quality-checked data from the LES site. A decrease of both fractions with the relative air mass is observed implying that the longer the path in the atmosphere, the greater the attenuation of the UV components relative to broadband GHI. The gentle decrease of f_{UVA} can be related to Rayleigh scattering in the atmosphere (which affects predominantly

short-wave photons) while Ozone absorption may explain the more prominent decrease in f_{UVB}. High [O_3] concentrations (in green) are associated to the lower portion of the f_{UVB} curves but do not significantly affect UVA. The dependence on k_t reflects the role of cloudiness (low k_t values are associated with cloudy conditions). Both UV fractions tend to increase for low k_t. These characteristics have been previously reported elsewhere (Foyo-Moreno, 1997; Murillo, 2003).

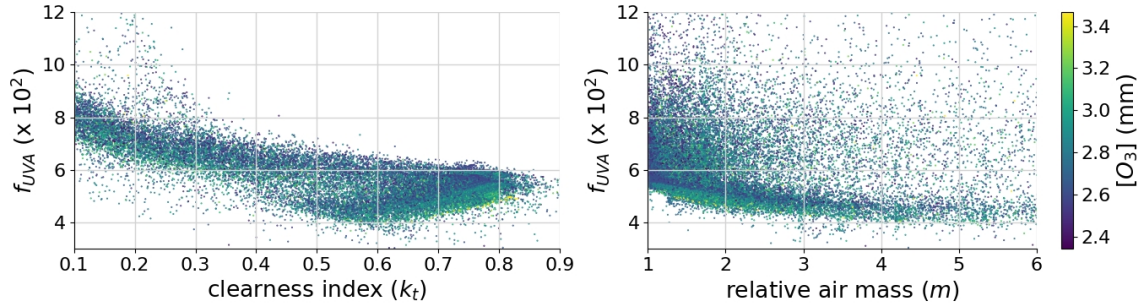

(a)

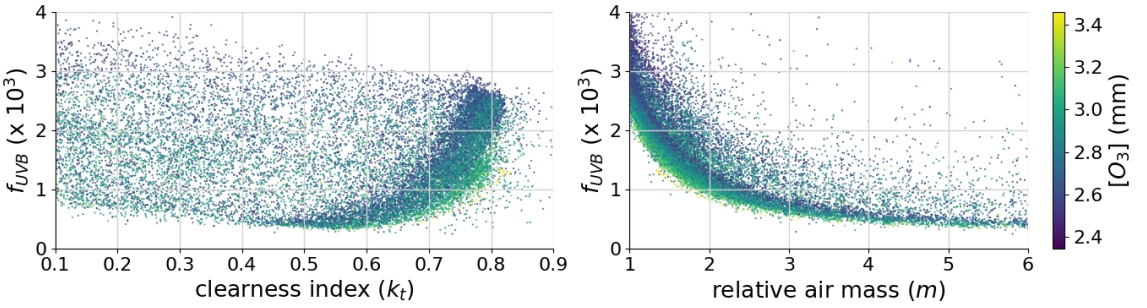

(b)

Fig.1: UV fraction vs clearness index and air mass (data from LES site). (a) UV-A fraction and (b) UV-B fraction are shown. Data is colored according to Ozone concentration, [O_3]. The dependence of f_{UVB} with Ozone concentration appears clearly. The behavior of f_{UVE} is similar to f_{UVB} (not shown).

2.2 Models

Several parametrizations for the UV fraction of each band (A, B, E) are considered and arranged in three families as described in Table 2. The clearness index, k_t, the relative optical air mass m and (for UV-B and UV-E) the Ozone column [O_3] are considered as predictor variables. We have tested that the inclusion of daily Ozone information does not provide a significant improvement for the UV-A band.

The different versions within each family correspond to a different dependence on the predictors. All the models can be obtained from those in Table 2, setting the relevant coefficients to zero according to Table 3. The constant model (F0) is included as the baseline model. It represents the average fraction for each UV sub-band at a given location. The F1 family corresponds to a simple polynomial parametrization (Martin and Goswami, 2005). The different versions within F1 correspond to the inclusion or not of air mass and Ozone in the model. The second family (F2) assumes a power law parametrization and has an underlying physical motivation (Martínez, 2007). The two versions in this class correspond to including or not Ozone in the UV-A model.

The third family (F3) describes an exponential parametrization which has proved useful in the context of diffuse fraction models (Abal et al, 2017) and is inspired on a generalized Lamber-Beer-Bougar law. Two variants (linear or quadratic in the exponent) are considered and two similar versions without Ozone are included for the UV-A band. In sum, aside from the baseline constant model, five models are tested in UV-A and four in the UV-B and UV-E bands, as summarized in Tables 2 and 3 below.

Table 2: Families of models for UV fraction. The coefficients a_i are locally adjusted and have different values for each model. $[O_3]$ the Ozone concentration in mm.

family	f_{UV}	# coefficients
F0	a_0	1
F1	$a_0 + a_1 k_t + a_2 k_t^2 + a_3 m + a_4 m^2 + a_5 [O_3] + a_6 [O_3]^2$	7
F2	$a_0\, k_t^{a1}\, m^{a2}\, [O_3]^{a3}$	4
F3	$a_0 \exp(a_1 k_t + a_2 k_t^2 + a_3 m + a_4 m^2 + a_5 [O_3] + a_6 [O_3]^2)$	7

Table 3: Individual models for UV fraction.

model	a_0	a_1	a_2	a_3	a_4	a_5	a_6	Band	#coefs
F0	·	na	na	na	na	na	na	all	1
$F1_1$	·	·	·	0	0	0	0	UVA	3
$F1_2$	·	·	·	·	·	0	0	UVA	5
$F1_{2oz}$	·	·	·	·	·	·	·	UVB, UVE	7
$F2_1$	·	·	·	0	na	na	na	UVA	3
$F2_{1oz}$	·	·	·	·	na	na	na	UVB, UVE	4
$F3_1$	·	·	0	·	0	0	0	UVA	3
$F3_{1oz}$	·	·	0	·	0	·	0	UVB, UVE	4
$F3_2$	·	·	·	·	·	0	0	UVA	5
$F3_{2oz}$	·	·	·	·	·	·	·	UVB, UVE	7

The model parameters are adjusted using standard linear and non-linear regression routines in Python and their performance is tested using a standard randomized cross-validation procedure in which half of the available data is randomly selected and used to train the model coefficient and the other half is used to obtain the performance indicators. This procedure (adjustment+evaluation) is repeated 1000 times, thus testing the repeatability and stability of the adjustment method. The average values of the metrics is reported in the next section. In Tabs. A.1, A.2 and A.3 (Appendix A) the average fitted parameters obtained for each model and site are shown for the UV-A, UV-B and UV-E bands, respectively.

The performance of each model is quantified by three indicators: the relative mean bias deviation (rMBD), the relative root mean square deviation (rRMSD) and the Kolmogorov-

Smirnoff Index (KSI), all expressed as a percentage of the corresponding measurement average. Each of these parameters tests different aspects of the agreement between the measured and estimated values (Gueymard, C., 2014; Espinar et al, 2009). A combined relative parameter

$$\kappa = \frac{1}{3}\left(|rMBD| + rMSD + KSI\right) \quad (1)$$

is also computed in order to provide a simple overall performance index for each model.

3. Models training and performance

The performance assessment of the locally adjusted UV models is described in this section. The metrics for each model performance are shown in Table 4. For each site and band, the ground measurements average (to which all relative indicators are referred as %) and the number of data pairs used in the validation are shown. The best performing models are

Table 4: Validation of model estimations vs ground measurements for each UV sub-band. All indicators are in % of the relevant measurement average (shown below). The number N_d of 15-min data pairs used for the comparison is also indicated for each site.

	UVA models						UVB models					UVE models				
	F0	**$F1_1$**	**$F1_2$**	**$F2_1$**	**$F3_1$**	**$F3_2$**	**F0**	**$F1_{2oz}$**	**$F2_{1oz}$**	**$F3_{1oz}$**	**$F3_{2oz}$**	**F0**	**$F1_{2oz}$**	**$F2_{1oz}$**	**$F3_{1oz}$**	**$F3_{2oz}$**
	BCA															
rMBD	-6.1	0.5	-0.2	-0.2	-0.9	**-0.1**	1.8	**0.2**	-0.6	-2.6	-1.0	-1.2	**-0.1**	-1.0	-2.5	-1.0
rRMSD	16.1	8.4	**7.9**	8.1	8.7	**7.9**	36.9	10.8	9.4	10.6	**9.1**	29.4	9.3	9.1	10.7	**8.9**
KSI	9.3	1.6	**0.8**	1.0	2.0	**0.8**	9.5	2.5	**1.5**	5.3	2.8	4.5	**2.2**	**2.2**	5.6	3.0
κ	10.5	3.5	**3.0**	3.1	3.9	**3.0**	16.1	4.5	**3.8**	6.2	4.3	11.7	**3.9**	4.1	6.3	4.3
mean #data	14.0 W/m^2; N_d = 4956						mean: 0.36 W/m^2; N_d = 5552					mean: 0.043 W/m^2; N_d = 5552				
	DNM															
rMBD	not applicable						10.8	**0.1**	-0.6	-2.2	-1.0	10.7	**+0.1**	-0.5	-2.2	-1.0
rRMSD							41.8	14.3	**9.5**	10.7	9.8	41.8	14.4	**9.5**	10.7	9.8
KSI							23.2	4.6	**0.8**	3.7	1.9	16.4	3.6	**1.3**	4.6	2.5
κ							25.3	6.3	**3.8**	5.5	4.2	23.0	6.0	**3.8**	5.8	4.4
mean #data							0.89W/m^2; N_d = 84166					0.063 W/m^2; N_d = 84500				
	LES															
rMBD	-0.7	1.7	-0.2	**-0.1**	-0.7	-0.3	9.0	**0.1**	-0.2	-1.6	-0.6	6.1	**0.0**	-0.6	-1.9	-0.7
rRMSD	10.3	8.2	**5.6**	5.7	6.0	5.7	36.3	10.5	**6.7**	7.8	6.9	28.5	8.7	**6.2**	8.0	6.6
KSI	2.1	4.0	0.9	**0.7**	2.2	0.9	23.2	4.6	**0.8**	3.7	1.9	16.4	3.6	**1.3**	4.6	2.5
κ	4.4	4.6	**2.2**	**2.2**	3.0	2.3	22.8	5.1	**2.6**	4.4	3.1	17.0	4.1	**2.7**	4.8	3.3
mean #data	25.1 W/m^2 ; N_d = 40326						0.85 W/m^2 ; N_d = 19906					0.087 W/m^2 ; N_d = 32028				

highlighted in bold face. For the UV-B and UV-E bands, the $F2_{1oz}$ models are more accurate in terms of rRMSD and rKSI. rRMSD between 7 and 10% are obtained for this model. For the UV-A band, the $F1_2$, $F2_1$ and $F3_2$ perform similarly, with rRMSD between 6 and 8% and $F1_2$ performing slightly better in BCA and $F2_1$ at the LES site. The widely used constant UV fraction (F0 model) ranks last among models considered and is inadequate for most applications.

Fig. 2: F2 models estimates for the UV-A and UV-E bands vs time for a cloudy day and a clear day at the LE site.

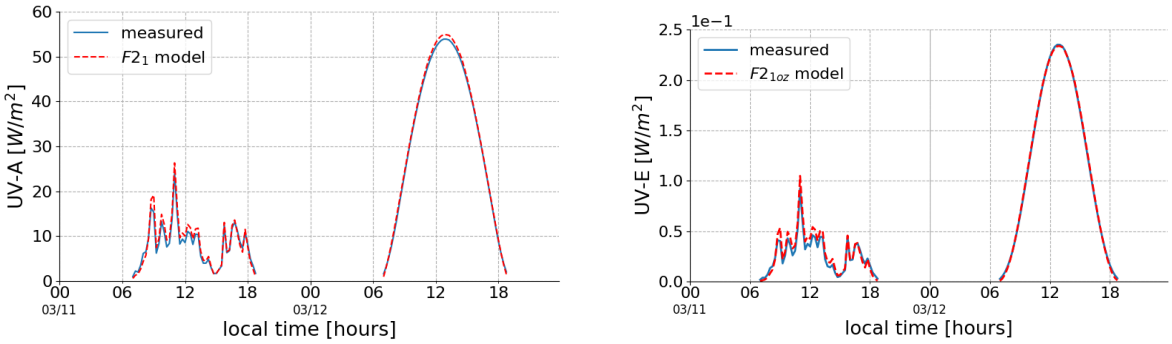

Fig. 2 shows the time series for models $F2_1$ and $F2_{1oz}$ for UV-A and UB-E bands at the LES site. An overcast and a clear day are shown and a good agreement is observed in both cases. A small underestimation around noon takes place in both bands, independently of cloud conditions. In Fig. 3, scatter plots for the best models for each band at different sites are shown: the $F1_2$ and $F2_1$ for UV-A, and $F2_{1oz}$ for the UV-B and UV-E bands. This effect can also be seen in Fig. 4, where the distributions of the rRMSD and rMBD indicators with k_t and the cosine of the solar zenith angle (z) are shown. At high values of *cos(z)* (or, equivalently, high solar altitude or low air masses) negative biases are observed in all bands. On the other hand, the rRMSD tends to be lower for high k_t values (clear sky) and higher at large values of *cos(z)* and low k_t (i.e. cloudy noons).

The performance of these simple models matches or overcomes the performance of similar models as reported in the literature, usually considering 30-minute or hourly estimates (which result in smoother data and lower indicators). The UV-A fraction average was found to be 5.6%, similar than the reported for locations with similar climate in Spain. On the other hand, at King's George Island (Antarctica) a slightly higher UV-A fraction of 7 % was measured, which can be explained by a higher frequency of cloudy conditions at this site. For the UV-B and UV-E bands, with the inclusion of daily Ozone information as a predictor, accurate estimates are obtained. The potential model ($F2_{1oz}$) is the best model at all sites, with exception of $F1_{2oz}$ which matches the performance of the former model for BCA site, specially in UV-E band. This model with daily OMI/TOMS Ozone information can successfully estimate the UV fraction with small bias and rRMSD around 7% (LES), and 9% (BCA), with a correlation above 0.995, a value which is close to the experimental uncertainty of the measurements. Constant fraction model F0 model is poorly accurate in B and E bands and its use should be avoided. Interestingly, mean UV-B and E fractions are lower in George King Island, Antarctica than in the country, in contrast to UV-A band.

Fig. 3: Scatter plots of the best models for each band. In the first row correspond to UV-A, the middle and bottom row corresponds to UV-B and UV-E respectively.

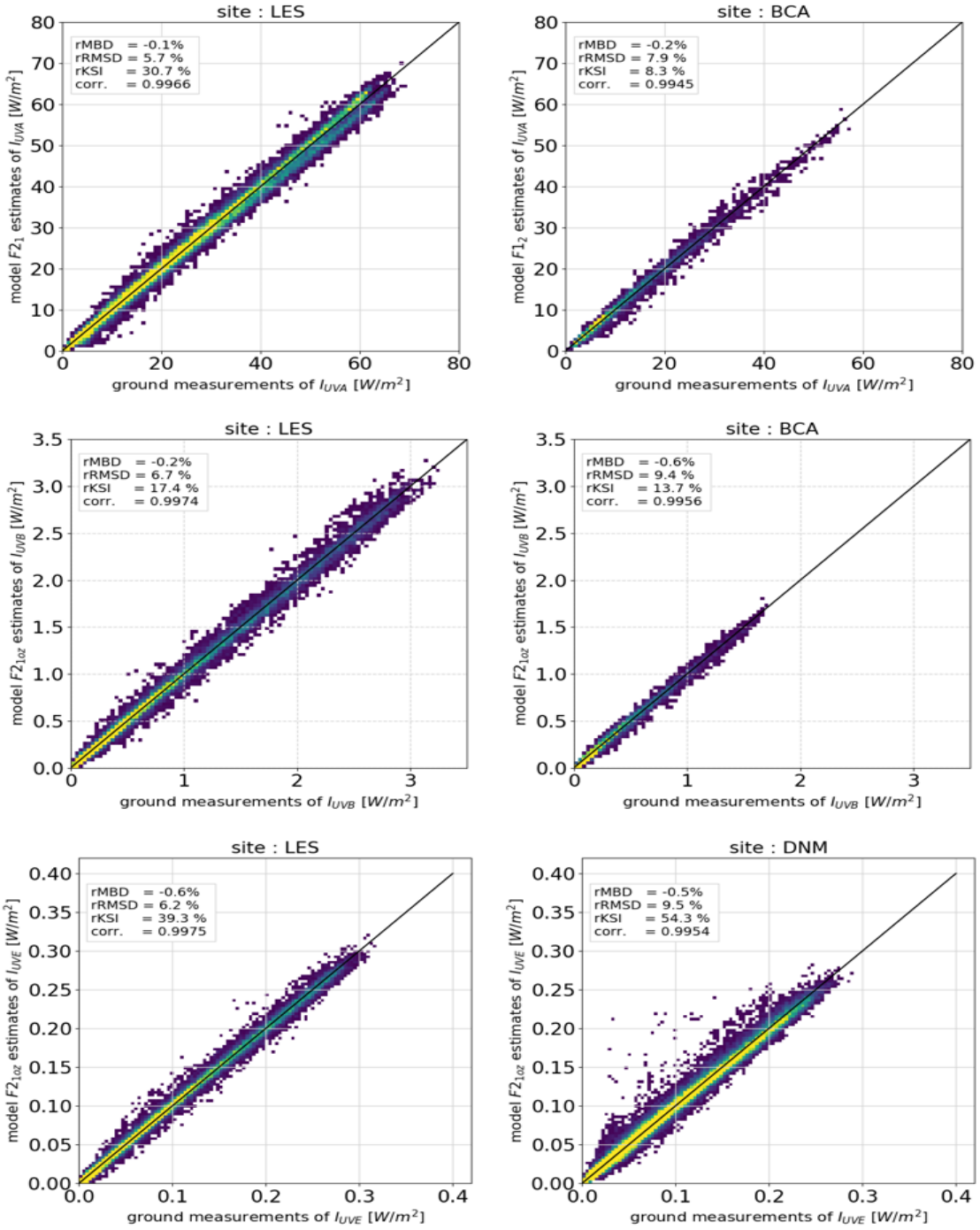

Considering factors such as the quality of the data, the performance for each model and the simplicity (as represented by the number of adjustable parameters), the F2 family of models provides the best description for all bands. The $F2_1$ model estimates UV-A with uncertainty under 6 % and negligible bias. With the inclusion of Ozone, $F2_{1oz}$ estimates UV-B and UV-E at LES (best data) with uncertainties of 6 and 7 %, respectively and small negative biases (under 0.6 %).

Fig. 4. rMBD (left) and rRMSD (right) distributions vs the cosine of the solar zenith angle and the clearness index at the LES site. Upper panels are for the to UV-A band and the lower panels for UV-E estimates.

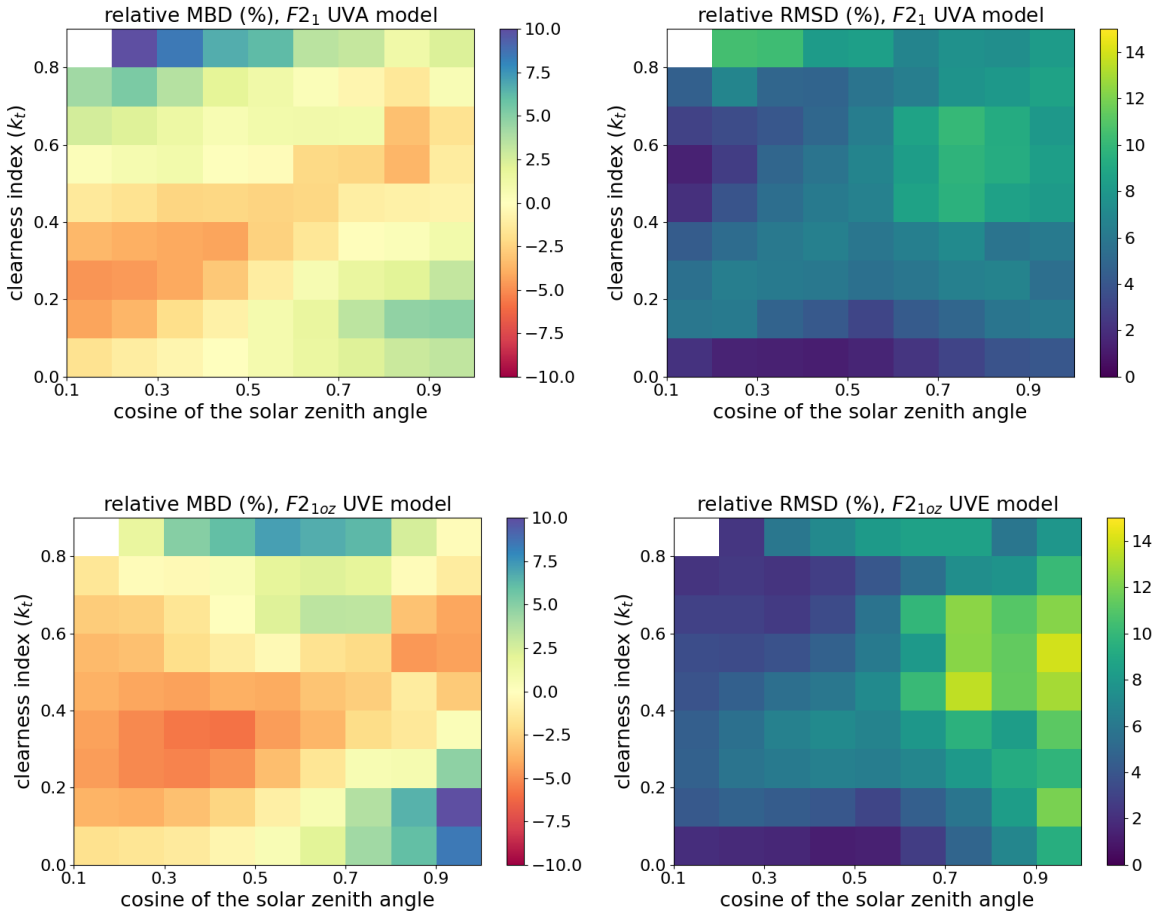

4. Summary and Conclusion

This study is the first UV radiation model evaluation performed over the Uruguayan territory and is part of a larger program which ultimately, aims to to map the spatial distribution of typical UV doses over the territory. It is based on reliable ground data collected at three sites (one of them close to the Antarctic circle) and for three UV bands (UV-A, UV-B and UV-E). All the data was integrated at the 15 minute level. Three families of empirical models that estimate the fraction of UV irradiance of GHI using clearness index, relative air mass and ozone density as predictors are considered. Random sampling and cross-validation techniques were used to assure statistical independence between the training and evaluation data sets.

These results show that the three families have locally adjusted models capable of good accuracy and low biases for all sub-bands and shows that the chosen set of predictors is adequate. Daily average atmospheric Ozone concentration is required for the UV-B and UV-E bands, but not relevant in the UV-A band. In this band, models $F1_2$, $F2_1$ and $F3_2$ are essentially equivalent in terms of performance. The UV-A fraction can be estimated with rRMSD in the range of 6 % (LES) to 8 % (BCA) of the average of the measurements and small negative biases. At the UV-B and UV-E bands, with the inclusion of Ozone concentration, UV irradiance can be estimated with rRMSD between 9 and 10 % and small biases. The best performance for all models is obtained at the LES site, which is the data of

best quality. The widely used constant UV fraction (F0 model) ranks last among models considered and is inadequate for most applications. The performance of these simple models matches or overcomes the performance of similar models as reported in the literature, usually considering 30-minute or hourly estimates.

Taking account the accuracy and simplicity the potential model (F2) is recommended for UV fraction modeling in all bands. At the LES site, these models estimate all bands with uncertainties between 6 and 7 % and small but consistently negative biases. These underestimation takes place mostly at low-medium k_t and high air mass (i.e low sun and cloudy conditions) and medium-high k_t and small air masses (i.e. high sun and clear-sky). The dispersion (in terms or rRMSD) is lower for air masses above 2 and tends to increase for smaller air mass.

This work shows that it is viable to model UV irradiance with uncertainties in the range 6-9% using simple (but locally adjusted) models based on clearness index, air mass and satellite-based Ozone concentration. This is a first step in a broader program which aims to generate reliable information on the UVA, UVB and UVE irradiation's typical spatial distributions, temporal variability and, ultimately, characterize the potential for daily UV exposure in the territory of Uruguay.

5. Acknowledgments

The authors thank the National Meteorological Institute (Uruguay) and specially Sergio Arizcorreta for the technical set-up, maintenance and management of the UV measurements at the DNM site.

6. References

Abal, G., Aicardi, D., Alonso Suárez, R., Laguarda, A., 2017. Solar Energy, 141, 166–181.

Alonso-Suárez, R., Abal, G., Siri, R., Musé, P., 2012. Brightness-dependent Tarpley model for global solar radiation estimation using GOES satellite images: application to Uruguay. Solar Energy Journal, 86(11), 3205–3215.

ACS (2019), American Cancer Society. Facts & Figures. American Cancer Society. Atlanta, Georgia, USA https://www.cancer.org/cancer/melanoma-skin-cancer/about/key-statistics.html Accessed 30/07/2019.

Calbó, J., Pagès, D.,, González, J. A., 2005. Empirical studies of cloud effects on UV radiation: A review. Reviews of Geophysics, 43, RG2002.

Cañada, J., Pedros, G. and Bosca, J.V., 2003. Relationships between UV (0.290–0.385 μm) and broad band solar radiation hourly values in Valencia and Córdoba, Energy 28, 199–217.

Espinar, B., Ramírez, L., Drews, A., Beyer, H. G., Zarzalejo, L. F., Polo, J.., Martín, L., 2009. Analysis of different comparison parameters applied to solar radiation data from satellite and German radiometric stations. Solar Energy 83, 118–125.

Foyo-Moreno, I., Vida, J. and Alados-Arboledas, L., 1997. Ground based ultraviolet (290 – 385 nm) and broadband solar radiation measurments in South-Eastern Spain.

Foyo-Moreno, I., Vida, J. and Alados-Arboledas, L., 1998. A Simple All Weather Model to Estimate Ultraviolet Solar Radiation (290–385 nm). Journal of applied meteorology, 38, 1020–1026.

Foyo-Moreno, I., Alados, I. and Alados-Arboledas, L., 2007. Adaptation of an empirical model for erythemal ultraviolet irradiance. Ann. Geophys., 25, 1499–1508.

Gueymard. C. 2014. A review of validation methodologies and statistical performance indicators for modeled solar radiation data: Towards a better bankability of solar projects, Renewable and Sustainable Energy Reviews, 39, 1024-1034.

ISO17166 (1999)/CIE S 007/E-1998: Erythema Reference Action Spectrum and Standard Erythema Dose. International Standarization Organization.

Laguarda, A., Alonso-Suárez, R., and Abal, G., 2018. Modelo semi-empírico de irradiación solar global a partir de imágenes satelitales GOES. Anais do VII Congresso Brasileiro de Energia Solar (CBENS2018), volume Radiação. ISBN 978-85-62179-02-0.

Lindfors, A., Kaurola, J., Arola, A., Koskela, T., Lakkala, K., Josefsson, W., , Olseth, J.A., Johnsen, B., 2007. A method for reconstruction of past UV radiation based on radiative transfer modeling: Applied to four stations in northern Europe. Journal of geophysical research, 112, D23201.

Martin, C.L. and Goswami, D.Y., 2005, Solar Energy Pocket Reference, ISES Booklet, ISBN 0-9771282-0-2.

Murillo, W., Cañada, J., Pedrós, G., 2003. Correlation between global ultraviolet (290–385nm) and global irradiation in Valencia and Cordoba (Spain). Renewable Energy, 28, 409–418.

Martínez, M.A., 2007. Doctoral dissertation at Universidad de Extremadura. https://documat.unirioja.es/descarga/tesis/1310.pdf. Accessed 18/3/2019.

Pawan, K. Bhartia, 2012, Goddard Earth Sciences Data and Information Services Center (GES DISC), Accessed: December 2018.

TOMS Science Team (Unrealeased), Goddard Earth Sciences Data and Information Services Center (GES DISC), Accessed: December 2018.

WMO/GAW (2014). Rationalizing nomenclature for UV doses and effects on humans. Report No.211 - CIE 209 World Meteorological Organization. Also WMO (2008). Guide to meteorological instruments and methods of observation. World Meteorological Organization, Geneva, Switzerland, seventh edition.

Young, A.T., 1994. Air-mass and refraction. Applied Optics, vol. 33, 1108-1110.

7. Appendix

For completeness, the locally adjusted parameters for each site and model are given below.

Table A.1: Adjusted parameters for each UVA model.

UVA	LES						BCA					
	F0	**$F1_1$**	**$F1_2$**	**$F2_1$**	**$F3_1$**	**$F3_2$**	**F0**	**$F1_1$**	**$F1_2$**	**$F2_1$**	**$F3_1$**	**$F3_2$**
a_0	5.6e-2	9.1e-2	9.8e-2	5.4e-2	9.3e-2	1.1e-1	7.0e-2	1.0e-1	1.2e-1	5.9e-2	9.9e-2	1.3e-1
a_1	–	-9.4e-2	-6.1e-2	-2.4e-1	-4.8e-1	-8.9e-1	–	-9.9e-2	-1.1e-1	-2.7e-1	-6.3e-1	-1.3
a_2	–	6.2e-2	2.8e-2	-2.0e-1	–	3.6e-1	–	5.8e-2	6.1e-2	-9.0e-2	–	6.7e-1
a_3	–	–	-1.1e-2	–	-1.2e-1	-1.9e-1	–	–	-8.0e-3	–	-2.8e-2	-1.1e-1
a_4	–	–	1.0e-3	–	–	1.9e-2	–	–	1.0e-3	–	–	1.3e-2

Table A.2: Adjusted parameters for each UVB model.

UVB	LES					BCA					DNM				
	F0	**$F1_{2oz}$**	**$F2_{10z}$**	**$F3_{1oz}$**	**$F3_{2oz}$**	**F0**	**$F1_{2oz}$**	**$F2_{1oz}$**	**$F3_{1oz}$**	**$F3_{2oz}$**	**F0**	**$F1_{2oz}$**	**$F2_{1oz}$**	**$F3_{1oz}$**	**$F3_{2oz}$**
a_0	2.0e-3	9.5e-3	7.6e-3	2.5e-2	6.1e-2	1.6e-3	6.8e-3	7.7e-3	1.8e-2	8.6e-2	2.3e-3	8.8e-3	9.0e-3	2.9e-2	7.3e-2
a_1	–	-1.9e-3	-2.3e-1	-4.6e-1	-7.0e-1	–	-2.0e-3	-3.2e-1	-6.8e-1	-9.9e-1	–	-1.8e-3	-1.5e-1	-3.0e-1	-6.6e-1
a_2	–	7.2e-4	-1.2	–	2.1e-1	–	6.8e-4	-1.2	–	2.8e-1	–	8.7e-4	-1.4	–	3.2e-1
a_3	–	-2.1e-3	-1.1	-8.6e-1	-1.2	–	-1.4e-3	-1.1	-6.1e-1	-9.7e-1	–	-2.6e-3	-1.1	-9.8e-1	-1.4
a_4	–	2.4e-4	–	–	1.1e-1	–	1.4e-4	–	–	8.6e-2	–	3.1e-4	–	–	1.3e-1
a_5	–	-2.2e-3	–	-3.9e-1	-8.0e-1	–	-1.1e-3	–	-3.2e-1	-1.1	–	-1.1e-3	–	-3.7e-1	-7.7e-1
a_6	–	2.5e-4	–	–	7.3e-2	–	1.1e-4	–	–	1.2e-1	–	5.4e-5	–	–	

Table A.3: Adjusted parameters for each UVE model.

UVE	LES					BCA					DNM				
	F0	**$F1_{2oz}$**	**$F2_{10z}$**	**$F3_{1oz}$**	**$F3_{2oz}$**	**F0**	**$F1_{2oz}$**	**$F2_{1oz}$**	**$F3_{1oz}$**	**$F3_{2oz}$**	**F0**	**$F1_{2oz}$**	**$F2_{1oz}$**	**$F3_{1oz}$**	**$F3_{2oz}$**
a_0	2.1e-4	8.3e-4	5.8e-4	1.6e-3	3.8e-3	1.9e-4	5.1e-4	4.7e-4	9.4e-4	1.7e-3	1.6e-4	6.2e-4	6.3e-4	2.0e-3	5.1e-3
a_1	–	-2.0e-4	-2.3e-1	-4.7e-1	-7.4e-1	–	-2.5e-4	-3.2e-1	-6.7e-1	-1.1	–	-1.3e-4	-1.5e-1	-3.0e-1	-6.9e-1
a_2	–	7.9e-5	-9.4e-1	–	2.3e-1	–	1.0e-4	-8.1e-1	–	3.5e-1	–	6.4e-5	-1.4e	–	3.3e-1
a_3	–	-1.7e-4	-8.6e-1	-6.4e-1	-9.4e-1	–	-1.2e-4	-6.4e-1	-4.0e-1	-6.9e-1	–	-1.8e-4	-1.1	-9.8e-1	-1.4
a_4	–	2.0e-5	–	–	9.5e-2	–	1.2e-5	–	–	6.5e-2	–	2.2e-5	–	–	1.3e-1
a_5	–	-1.7e-4	–	-3.0e-1	-7.2e-1	–	-6.5e-7	–	-1.8e-1	-2.6e-1	–	-7.8e-5	–	-3.7e-1	-7.6e-1
a_6	–	1.9e-5	–	–	7.4e-2	–	-5.5e-6	–	–	8.8e-3	–	3.9e-6	–	–	6.8e-2